ACCURACY CRITERION FOR SOURCE POWER INTEGRATION WITH CSM DIAGONAL REMOVAL

Pieter Sijtsma[1,2]
[1]PSA3, Prinses Margrietlaan 13, 8091 AV, Wezep, The Netherlands
[2]Faculty of Aerospace Engineering, TU Delft, The Netherlands

ABSTRACT

In this paper an accuracy criterion is derived for acoustic array measurements that are disturbed by incoherent noise, for example turbulent boundary layer noise in a wind tunnel. The accuracy criterion is a minimum signal-to-noise ratio at which the output of the array processing method has at least 95% likelihood of being within 1 dB error. Array processing is done with source power integration methods applied to cross-spectral matrices without diagonal. The integrated results are scaled to average microphone data and can therefore be considered as denoised array data. This paper derives the accuracy criterion for broadband noise signals consisting of multiple plane waves and for a line source of zero coherence length. For both cases, the validity of the criterion is confirmed with synthesized broadband noise array data.

NOMENCLATURE

CB	Conventional Beamforming
CSM	Cross-Spectral Matrix
DFT	Discrete Fourier Transform
ISPI	Inverse SPI
PSF	Point Spread Function
RMS	Root-Mean-Square
SNR	Signal-to-Noise Ratio
SPI	Source Power Integration
SPIL	SPI with Line source
TBL	Turbulent Boundary Layer
TE	Trailing Edge
A	source power estimate
$\bar{A}$	source power, $E\{A\}$
a	source amplitude
B_{kl}	PSF, see Eq. (27)
b	noise
C_{mn}	cross-spectrum
c	sound speed
D	array diameter
$E\{\cdot\}$	expectation value
F	cost function
f	frequency
g	acoustic transfer function
J	number of averages
j	snapshot index
K	number of (equivalent) sources
k	source index
L	line length
l	source index
m	microphone index
N	number of microphones
n	microphone index

P	probability	Δf	frequency bandwidth
p	measured pressure	Θ^2	Noise-to-Signal Ratio
s	signal	κ	acoustic wave number, $2\pi f/c$
T	recorded time length	κ_x	spatial wave number
t	time	κ_y	spatial wave number
x	cartesian coordinate	κ_z	spatial wave number
y	cartesian coordinate	σ	standard deviation
Z	distance between array and line	σ^2	variance
z	cartesian coordinate	σ_0^2	= 0.013344

1 INTRODUCTION

Microphone signals can be severely distorted by wind noise. This is, for example, an issue when microphones are mounted in the wall of a closed wind tunnel test section or on the fuselage of an aircraft. Unsteady pressures due to turbulence in the boundary layer may be an order of magnitude higher than the noise radiated from the object under investigation. This issue is usually alleviated by using multiple microphones and combining the signals in a clever way. A lot of research has been performed recently [1-9] towards finding the best denoising technique, if possible taking advantage of the low rank of the signal part of the Cross-Spectral Matrix (CSM) or using knowledge about the origin of the acoustic sources.

A notorious denoising challenge concerns airfoil measurements in a closed test section of a wind tunnel, where the aim is to separate airfoil Trailing Edge (TE) noise from other noise measured by wall-mounted microphones. The levels of TE noise radiating from an airfoil are much lower than the pressure levels underneath a Turbulent Boundary Layer (TBL), with Signal-to-Noise Ratio (SNR) typically below −40 dB.

For denoising airfoil TE noise measurements, beamforming is the only option, as low-rank CSM reconstruction techniques [1,6,7] do not apply. Beamforming methods benefit from CSM diagonal removal, since the microphone signals can usually be considered mutually incoherent. However, CSM diagonal removal is far from sufficient. Too much noise remains in the cross-spectra, which can only be reduced sufficiently with unrealistically long recording times. In other words, TE noise measurements with microphones mounted flush in wind tunnel walls are doomed to fail.

A possible solution to perform, nevertheless, successful TE noise measurements in a closed wind tunnel test section is recessing the microphones in cavities covered by an acoustically transparent sheet like a wire mesh or Kevlar [10-14]. These devices take advantage of the short hydrodynamic wave lengths of TBL pressures, which are evanescent inside the cavity. Thus, the SNR can increase significantly, up to 30 dB. Herewith, TE noise measurements in closed test section wind tunnels become feasible, thus providing an alternative for a set-up with Kevlar walls [15,16].

The application limits of such measurements depend on the number of microphones, the length of the recording time, the remaining background noise level in the cavities and the noise emitted from the airfoil TE. The aim of this paper is to provide a prediction formula to predict the minimum SNR at which beamforming results are still reliable, i.e., the TE noise floor levels for given TBL noise levels. This expression provides insight into the feasibility of wind tunnel measurements for a given airfoil and can set targets for optimising the cavities.

To derive such a formula, we assume that TE edge noise can be represented by a line source with zero correlation length. In practice, the correlation length is finite, but much smaller than what can be detected by a microphone array.

The paper starts with deriving an expression for the simpler case of isolated far-field sources (i.e., plane waves). This will be done in Chapter 2. In Chapter 3, the line source is considered. The validity of the minimum SNR prediction is demonstrated with synthesized array measurements. Conclusions follow in Chapter 4.

2 FAR-FIELD SOURCES

2.1 Single source

Consider an array of N microphones. Let the signal measured by microphone n be

$$p_n(t) = s_n(t) + b_n(t), \tag{1}$$

where $s_n(t)$ is a broadband noise signal from a source far away (plane wave) and $b_n(t)$ incoherent noise with microphone independent statistical properties. The Fourier transform is applied to a range of time intervals (snapshots). For fixed frequency and for a single snapshot, the (complex valued) Fourier transform of Eq. (1) is written as

$$p_{n,j} = s_{n,j} + b_{n,j}, \tag{2}$$

with j the snapshot index. The CSM is obtained by averaging over J snapshots:

$$C_{mn} = \frac{1}{J}\sum_{j=1}^{J}\left(s_{m,j} + b_{m,j}\right)\left(s_{n,j}^* + b_{n,j}^*\right), \tag{3}$$

where the asterisk denotes complex conjugation. The signal is assumed to be a plane wave coming from a certain direction, that is

$$s_{n,j} = a_j g_n, \tag{4}$$

with $|g_n| = 1$.

The amplitudes a_j and $b_{n,j}$ are assumed to be complex Gaussian random variables with expectation value zero. The variances are

$$\sigma^2(a_j) = E\left\{|a_j|^2\right\} = \lim_{J\to\infty}\frac{1}{J}\sum_{j=1}^{J}|a_j|^2 = \bar{A} = 1, \tag{5}$$

$$\sigma^2(b_{n,j}) = E\left\{|b_{n,j}|^2\right\} = \lim_{J\to\infty}\frac{1}{J}\sum_{j=1}^{J}|b_{n,j}|^2 = \Theta^2. \tag{6}$$

Hence, the SNR is $-10\log_{10}\left(\Theta^2\right)$. In other words, Θ^2 is the Noise-to-Signal Ratio.

Thus, the signal CSM to be retrieved is

$$C_{mn}^{\text{signal}} = \bar{A} g_m g_n^* = g_m g_n^*. \tag{7}$$

The average signal auto-power is

$$\frac{1}{N}\sum_{n=1}^{N} C_{nn}^{\text{signal}} = \frac{\bar{A}}{N}\sum_{n=1}^{N} g_n g_n^* = \bar{A} = 1. \tag{8}$$

An estimate A of $\bar{A}$ can be obtained with Conventional Beamforming (CB), which minimises the following cost function:

$$F = \sum_{m,n}\left|C_{mn} - A g_m g_n^*\right|^2, \tag{9}$$

yielding

$$A = \sum_{m,n} g_m^* C_{mn} g_n \Big/ \sum_{m,n} (1) . \tag{10}$$

In Eq. (10) we may sum over all (*m*,*n*)-combinations, but in this paper the diagonal elements $m = n$ are omitted:

$$A = \frac{1}{N(N-1)} \sum_{m,n} g_m^* C_{mn} g_n . \tag{11}$$

Equation (11) is the denoised average auto-power.

With the expressions above we can write

$$A = \frac{1}{J} \sum_{j=1}^{J} \left| a_j \right|^2 + \frac{1}{N(N-1)J} \left\{ \sum_{m,n} g_n \sum_{j=1}^{J} a_j b_{n,j}^* + \sum_{m,n} g_m^* \sum_{j=1}^{J} b_{m,j} a_j^* + \sum_{m,n} g_m^* g_n \sum_{j=1}^{J} b_{m,j} b_{n,j}^* \right\} . \tag{12}$$

For the expectation value we have

$$E\{A\} = 1 . \tag{13}$$

The variance of *A* is

$$\begin{aligned} \sigma^2(A) &= E\left\{ \left(A - \bar{A} \right)^2 \right\} = E\left\{ \left(A - 1 \right)^2 \right\} = E\left\{ \left(\frac{1}{J} \sum_{j=1}^{J} \left| a_j \right|^2 - 1 \right)^2 \right\} + \left(\frac{1}{N(N-1)J} \right)^2 \times \\ &\left[E\left\{ \left| \sum_{m,n} g_n \sum_{j=1}^{J} a_j b_{n,j}^* \right|^2 \right\} + E\left\{ \left| \sum_{m,n} g_m^* \sum_{j=1}^{J} a_j^* b_{m,j} \right|^2 \right\} + E\left\{ \left| \sum_{m,n} g_m^* g_n \sum_{j=1}^{J} b_{m,j} b_{n,j}^* \right|^2 \right\} \right] \\ &= \frac{1}{J} + \left(\frac{1}{N(N-1)J} \right)^2 \left[N(N-1)^2 J\Theta^2 + N(N-1)^2 J\Theta^2 + N(N-1) J\Theta^4 \right] \\ &= \frac{1}{J} \left(1 + \frac{2\Theta^2}{N} + \frac{\Theta^4}{N(N-1)} \right) . \end{aligned} \tag{14}$$

The evaluation of the first term is a special case ($K = 1$ and $\bar{A} = 1$) of Appendix A.

For given variance $\sigma^2(A)$ (or standard deviation σ) the probability of making an error less than 1 dB is

$$P(\sigma^2) = \frac{1}{\sigma\sqrt{2\pi}} \int_{10^{-0.1}}^{10^{0.1}} \exp\left(-\frac{(\xi - 1)^2}{2\sigma^2} \right) d\xi = \frac{1}{2} \left(\mathrm{Erf}\left(\frac{10^{0.1} - 1}{\sigma\sqrt{2}} \right) + \mathrm{Erf}\left(\frac{1 - 10^{-0.1}}{\sigma\sqrt{2}} \right) \right) . \tag{15}$$

For $\sigma^2 = 0.013344$ we have $P(\sigma^2) = 0.95$. In other words, if

$$\sigma^2(A) = \frac{1}{J} \left[1 + \frac{2\Theta^2}{N} + \frac{\Theta^4}{N(N-1)} \right] \le \sigma_0^2 = 0.013344 \tag{16}$$

or, equivalently,

$$\Theta^2 \le (N-1) \left[-1 + \sqrt{1 - \frac{N}{N-1} \left(1 - \sigma_0^2 J \right)} \right] , \tag{17}$$

then the probability of making an error less than 1 dB is more than 95%. Obviously, a different percentage and a different tolerance would yield a different value for σ_0^2.

If the errors are small, the relation between errors in dB and $\sigma^2(A)$ is

$$\sigma^2\left(\Delta\,\mathrm{dB}\right)=\left(\frac{10}{\ln\left(10\right)}\right)^2\sigma^2\left(A\right). \tag{18}$$

Hence, the standard deviation of the spectrum with $\sigma^2\left(A\right)=\sigma_0^2$ is

$$\sigma\left(\Delta\,\mathrm{dB}\right)=\frac{10}{\ln\left(10\right)}\sqrt{0.013344}=0.50168\ \mathrm{dB}\,. \tag{19}$$

2.2 Multiple sources

Now assume there are *K* incoherent sources:

$$p_{n,j}=\sum_{k=1}^{K}a_{k,j}g_{k,n}+b_{n,j}\,. \tag{20}$$

The variances of $a_{k,j}$ may be *k*-dependent:

$$\sigma^2\left(a_{k,j}\right)=\bar{A}_k\,. \tag{21}$$

They are scaled through

$$\sum_{k=1}^{K}\bar{A}_k=1, \tag{22}$$

which means that Θ^2 of Eq. (6) still represents the Noise-to-Signal Ratio. For the CSM we have

$$C_{mn}=\frac{1}{J}\sum_{j=1}^{J}\left(\sum_{k=1}^{K}a_{k,j}g_{k,m}+b_{m,j}\right)\left(\sum_{k=1}^{K}a_{k,j}^{*}g_{k,n}^{*}+b_{n,j}^{*}\right). \tag{23}$$

The equivalent of Eq. (9) is

$$F=\sum_{m,n}\left|C_{mn}-\sum_{k=1}^{K}A_k g_{k,m}g_{k,n}^{*}\right|^2, \tag{24}$$

which can be solved with a standard Non-Negative Least Squares solver [17]. This procedure is basically the Inverse Source Power Integration (ISPI) approach of Merino-Martínez et al. [18]. The denoised auto-power is now

$$A=\sum_{k=1}^{K}A_k\,. \tag{25}$$

If the source powers A_k are all positive, then the derivatives of *F* are zero, yielding

$$\sum_{l=1}^{K}B_{kl}A_l=\sum_{m,n}g_{k,m}^{*}C_{mn}g_{k,n},\ k=1,\ldots,K\,, \tag{26}$$

with

$$B_{kl}=\sum_{m,n}g_{k,m}^{*}g_{l,m}g_{l,n}^{*}g_{k,n}\,. \tag{27}$$

This is basically the DAMAS [19] problem, with B_{kl} the Point Spread Function (PSF). If the sources are well-separated (not in each other's main lobe) and if the array is well designed (low side lobe levels), then B_{kl} may be assumed negligible for $k\neq l$, yielding

$$A_k=\frac{1}{N\left(N-1\right)}\sum_{m,n}g_{k,m}^{*}C_{mn}g_{k,n}\,, \tag{28}$$

which is CB for the individual sources (Eq. (11)). Then, the denoised auto-power is

$$A = \frac{1}{N\left(N-1\right)} \sum_{k=1}^{K} \sum_{m,n} g_{k,m}^{*} C_{mn} g_{k,n} \,, \tag{29}$$

which is the ordinary Source Power Integration (SPI) method.

Under the above-mentioned assumptions for SPI, we have $E\{A\} = 1$. Furthermore, analogously to Eq. (14) we have

$$\begin{aligned} \sigma^2(A) = E\left\{\left(\frac{1}{J}\sum_{k=1}^{K}\sum_{j=1}^{J}\left|a_{k,j}\right|^2 - 1\right)^2\right\} + \left(\frac{1}{N(N-1)J}\right)^2 \left[E\left\{\left|\sum_{k=1}^{K}\sum_{m,n} g_{k,n}\sum_{j=1}^{J} a_{k,j} b_{n,j}^{*}\right|^2\right\} \right. \\ \left. + E\left\{\left|\sum_{k=1}^{K}\sum_{m,n} g_{k,m}^{*}\sum_{j=1}^{J} a_{k,j}^{*} b_{m,j}\right|^2\right\} + E\left\{\left|\sum_{k=1}^{K}\sum_{m,n} g_{k,m}^{*} g_{k,n}\sum_{j=1}^{J} b_{m,j} b_{n,j}^{*}\right|^2\right\}\right], \end{aligned} \tag{30}$$

further evaluated to

$$\sigma^2(A) = \frac{1}{J}\left(\sum_{k=1}^{K} \bar{A}_k^2 + \frac{2\Theta^2}{N} + \frac{K\Theta^4}{N\left(N-1\right)}\right). \tag{31}$$

For the evaluation of the first term, the reader is referred to Appendix A. Analogously to Eq. (17), the 1 dB criterion is now

$$\Theta^2 \le \frac{N-1}{K}\left(-1 + \sqrt{1 - \frac{NK}{N-1}\left(\sum_{k=1}^{K} \bar{A}_k^2 - \sigma_0^2 J\right)}\right). \tag{32}$$

It can be shown that

$$\frac{1}{K} \le \sum_{k=1}^{K} \bar{A}_k^2 \le 1 \,. \tag{33}$$

Therefore, if the source powers $\bar{A}_k$ are unknown, we can replace Eq. (32) by the bit more conservative criterion:

$$\Theta^2 \le \frac{N-1}{K}\left(-1 + \sqrt{1 - \frac{NK}{N-1}\left(1 - \sigma_0^2 J\right)}\right). \tag{34}$$

2.3 Simulations

Array measurements were synthesized with an array in the $z = 0$ plane, consisting of $N = 93$ microphones within a circular aperture of $D = 2$ m diameter. The layout of the microphones, shown in Fig. 1, is the same as used in [8]. For each microphone, $T = 60$ s of time data was synthesized at 25 kHz sample rate. Noise and signal data were generated separately and summed afterwards.

Time data were generated by convolving sampled Gaussian white noise data (all samples independent) with a window function leading to the auto-spectrum shown in Fig. 2. The window function is basically the inverse Fourier transform of the square root of the targeted auto-spectrum. Noise was generated for each microphone separately, making the noise signals incoherent.

Spectra were calculated by averaging Fourier transformed data from snapshots of 500 samples, yielding a frequency resolution of $\Delta f = 50$ Hz. A rectangular DFT window was used, without overlap, so the number of averages was $J = 3000$. The difference between the

average noise auto-spectrum and the target auto-spectrum was very small: The Root-Mean-Square (RMS) deviation was 0.011 dB.

Additionally, signal data (plane waves) from $K = 5$ different directions were synthesized. The directions (relative spatial wave numbers) and relative levels are shown in Table 1. With these relative levels, we can evaluate the summation in Eq. (31):

$$\sum_{k=1}^{K} \bar{A}_k^2 = \sum_{k=0}^{4} 10^{-2k/10} \Bigg/ \left(\sum_{k=0}^{4} 10^{-k/10} \right)^2 = 0.221 . \tag{35}$$

The signal time data were generated similarly to the noise data, only the sample rate was increased to 100 kHz to facilitate interpolation at the microphone locations. The same target spectrum (Fig. 2) was used, but now extended with a constant value of −100 dB towards the Nyquist frequency (50 kHz). After summation, the signal was scaled to the level in Fig. 2.

Table 1. Wave numbers and relative levels of far-field sources

κ_x/κ	κ_y/κ	κ_z/κ	Relative SPL
0	0	1	0 dB
−0.2357	−0.2357	0.9428	−1 dB
−0.2357	0.2357	0.9428	−2 dB
0.2357	0.2357	0.9428	−3 dB
0.2357	−0.2357	0.9428	−4 dB

Thus, signal data $s(t)$ and noise data $b(t)$ were obtained with the same average auto-spectrum. Summed data were generated by

$$p(t) = s(t) + 10^{-\mathrm{SNR}/20} b(t) . \tag{36}$$

The denoised spectrum can be obtained from Eq. (25), with A_k values calculated by CB, Eq. (28), or by directly solving Eq. (24). This corresponds, respectively, with the SPI and the ISPI method described in [18]. The results are shown in Fig. 3. Starting from 700 Hz, the results of both methods are close to each other and close to the target spectrum. Apparently, the assumption of B_{kl} being small for $k \neq l$ holds for frequencies above 700 Hz. Since the results with ISPI are better, also above 700 Hz, we will proceed with ISPI.

The difference between ISPI and the target spectrum is shown in Fig. 4. The RMS value is $\Delta \mathrm{dB}_{\mathrm{rms}} = 0.040$ dB. This is close to the predicted standard deviation of 0.037 dB, which is found by combining Eqs. (18), (31) with $\Theta = 0$, and (35). There is, however, a small offset, probably explained by the fact that oblique waves do not simultaneously arrive at different microphones, causing a slight mismatch in snapshots when the CSM is calculated.

Equation (32) predicts a minimum SNR of -23.861 dB. The corresponding accuracy (difference between ISPI and target) is shown in Fig. 5. The RMS value is 0.495 dB, which is very close to the standard deviation predicted by Eq. (19). The number of frequency bands for which the error is more than 1 dB is 11. With 200 frequency bands, this is indeed approximately the expected 5% occurrences.

This simulation was repeated three times with new time data. The results, which yielded RMS values comparable to the first run, are summarised in Table 2.

Furthermore, using the time data of Run 1, denoising was done with ±2 dB added to the SNR. The results are summarised in Table 3 and demonstrate the sensitivity to SNR: results get quickly worse when the SNR decreases by 2 dB.

Table 2: Plane wave results with SNR = −23.861 dB

	$\Delta\mathrm{dB}_{\mathrm{rms}}$	$\#\ \lvert\Delta\mathrm{dB}\rvert > 1$
Run 1	0.495 dB	11
Run 2	0.531 dB	15
Run 3	0.431 dB	2
Run 4	0.522 dB	8

Table 3: Plane wave results with varying SNR (Run1 data)

SNR	$\Delta\mathrm{dB}_{\mathrm{rms}}$	$\#\ \lvert\Delta\mathrm{dB}\rvert > 1$
−21.861 dB	0.327 dB	1
−23.861 dB	0.495 dB	11
−25.861 dB	0.763 dB	29

3 LINE SOURCE

3.1 Equivalent sources

Next we consider a line source of length $L = 2$ m, located at $Z = 2$ m distance from the array. The Cartesian coordinates of the line are $x = 0$, $-1 \le y \le 1$ and $z = 2$. As stated in the Introduction, we represent the line source by a large number (500) of incoherent point sources with the same strength. Time data is generated analogously to the previous chapter: the source strength is tuned such that the average auto-spectrum at the array is equal to the target spectrum.

For two reasons, the theory of the previous chapter is not directly applicable. First, the assumption of far-field sources (plane waves) does not apply. Second (and most important), the assumption of B_{kl} being negligible for $k \neq l$ cannot hold with the sources so closely spaced.

The second shortcoming can be overcome by representing the line source by a finite number of equivalent point sources. The question is: by how many sources can the line be represented to obtain an accurate CSM? The answer to this question is frequency dependent.

A first attempt to answer this question is found by dividing the line length through the Rayleigh resolution limit $1.22cZ/Df$, where f is the frequency and c the sound speed. With this, the equivalent number of sources becomes

$$K = \frac{LDf}{1.22cZ}. \tag{37}$$

Another approach is to count the number of iterations that CLEAN-SC [20] (with unit loop gain) requires until the peak level of the "dirty map" is 10 dB below the peak level of the CB map. This check was done on measurements without noise. The resulting number of iterations per frequency band are compared with Eq. (37) in Fig. 6. There is a very good agreement, so Eq. (37) seems like an excellent starting point for estimating the number of equivalent sources. There is some arbitrariness, however, as the number of CLEAN-SC will be different if the threshold of −10 dB is set differently.

When the K equivalent sources have equal strength, then Eq. (22) yields

$$\bar{A}_k = \frac{1}{K} \tag{38}$$

and for Eq. (32) we obtain:

$$\Theta^2 \le \frac{N-1}{K}\left(-1+\sqrt{1-\frac{N}{N-1}\left(1-\sigma_0^2 JK\right)}\right). \tag{39}$$

3.2 1/3 octave bands

Insertion of Eq. (37) into Eq. (39) leads to a strongly frequency dependent SNR criterion. This frequency dependency can be suppressed by considering 1/3 octave frequency bands. The number of averages per 1/3 octave band can be estimated with the bandwidth-time product:

$$J \approx T\Delta f = f_{1/3\text{-octave}}\left(10^{0.05}-10^{-0.05}\right)T\,. \tag{40}$$

With Eqs. (37), (39) and (40) we obtain a 1 dB criterion that is only weakly dependent on frequency. For the synthesized array data of this paper, the SNR values are plotted in Fig. 7. For a comparison similar to Section 2.3, we will use the value at 1000 Hz.

3.3 Simulations

Synthesized data for the line source were obtained similarly to the far-field sources. The line is represented by 500 incoherent point sources of uniform directivity and equal strength. For each source, the pressure standard deviation decays proportionally with distance.

The source amplitude can be solved with Eq. (24). Since all sources have equal strength, this boils down to minimising

$$F = \sum_{m,n}\left|C_{mn} - A\sum_{k=1}^{K} g_{k,m}g_{k,n}^*\right|^2. \tag{41}$$

The solution is

$$A = \sum_{k=1}^{K}\sum_{m,n} g_{k,m}^* C_{mn} g_{k,n} \Bigg/ \sum_{k=1}^{K}\sum_{l=1}^{K} B_{kl}\,. \tag{42}$$

This is the SPIL method of [18], by which the best results were found for similar synthesized line source benchmark measurements [21]. The denoised average auto-power is then

$$\frac{1}{N}\sum_{n=1}^{N} C_{nn}^{\text{denoised}} = \frac{A}{N}\sum_{n=1}^{N}\sum_{k=1}^{K}\left|g_{k,n}\right|^2. \tag{43}$$

Table 4: Line source results with SNR = −27.433 dB

	$\Delta\text{dB}_{\text{rms}}$	$\#\ \lvert\Delta\text{dB}\rvert > 1$
Run 1	0.283 dB	0
Run 2	0.454 dB	1
Run 3	0.426 dB	0
Run 4	0.726 dB	3

At 1000 Hz, the theory predicts an SNR threshold of −27.433 dB. A typical error curve, for frequencies ranging from 200 to 8000 Hz is shown in Fig. 8. At each of the 17 frequencies, the error is within 1 dB. The RMS value is 0.283 dB, which is less than the predicted standard deviation of 0.502 dB (Eq. (19).

The equivalent of Table 2 (several runs) is shown in Table 4. The RMS values vary more than in Table 2, which is due to the lower number of frequency bands (17 instead of 200). But on average, the standard deviation is not so far from 0.5 dB. The total percentage of errors larger than 1 dB is 5.8%.

4 CONCLUSION

In this paper, expressions are derived to predict the minimum SNR at which denoised microphone data can be obtained with at least 95% likelihood of being within 1 dB accuracy. Denoising is done with source power integration methods described by Merino-Martínez et al. [18], with removal of the CSM diagonal. The predicted accuracy showed good agreement with synthesized data.

For convenience, the spectral analysis in this paper was done without using the Hanning window, usually applied to measured aeroacoustic data. The Hanning window can be considered as a moving average or smoothing function over the frequency bands. Therefore, the errors when using the Hanning window will be smaller than with a rectangular window, especially for the narrow-band results and for low-frequency 1/3 octave bands.

Source directivity, which is a typical feature of TE noise, is not included either. Dependent on the pattern of the directivity, this will lead to some reduction of SNR.

REFERENCES

[1] Q. Leclère, N. Totaro, C. Pézerat, F. Chevillotte, and P. Souchotte, “Extraction of the acoustic part of a turbulent boundary layer from wall pressure and vibration measurements”, NOVEM 2015: Noise and Vibration - Emerging Technologies, Dubrovnik, Croatia, 13-15 April 2015.

[2] A. Finez, A. Pereira, and Q. Leclère, “Broadband mode decomposition of ducted fan noise using Cross-Spectral Matrix denoising”, FAN 2015, Lyon, France, 15-17 April 2015.

[3] R.P. Dougherty, “Cross-Spectral Matrix diagonal optimization”, BeBeC-2016-S2, 6th Berlin Beamforming Conference, 29 February - 1 March 2016.

[4] J. Hald, “Cross-Spectral Matrix diagonal reconstruction”, Internoise 2016, Hamburg, Germany, 21-24 August 2016.

[5] C.J. Bahr, and W.C. Horne, “Subspace-based background subtraction applied to aeroacoustic wind tunnel testing”, Int. J. Aeroacoustics, 16 (4-5), 299-325, 2017.

[6] A. Dinsenmeyer, J. Antoni, Q. Leclère, and A. Pereira, “On the denoising of Cross-Spectral Matrices for (aero)acoustic applications”, BeBeC-2018-S02, 7th Berlin Beamforming Conference, 5-6 March 2018.

[7] A. Dinsenmeyer, Q. Leclère, J. Antoni, and E. Julliard, "Comparison of microphone array denoising techniques and application to flight test measurements", AIAA 2019-2744, 25th AIAA/CEAS Aeroacoustics Conference, Delft, The Netherlands, 20-23 May 2019.

[8] P. Sijtsma, A, Dinsenmeyer, J. Antoni, and Q. Leclère, “Beamforming and other methods for denoising microphone array data”, AIAA 2019-2653, 25th AIAA/CEAS Aeroacoustics Conference, Delft, The Netherlands, 20-23 May 2019.

[9] G. Jiang, C. Sun, and X. Liu, "Diagonal denoising for conventional beamforming via sparsity optimization", IEEE Access, 8, 11416-11425, 2020.
[10] A. Carballo-Crespo, and K. Takeda, "An investigation of microphone array installation effects", AIAA 2009-883, 47th AIAA Aerospace Sciences Meeting, Orlando, FL, 5-8 January 2009.
[11] V. Fleury, L. Coste, R. Davy, A. Mignosi, J.-M. Prosper, and C. Cariou, "Optimization of microphone array wall-mountings in closed-section wind tunnels", AIAA 2010-3738, 16th AIAA/CEAS Aeroacoustics Conference, Stockholm, Sweden, 7-9 June 2010.
[12] http://www.gras.dk/products/special-microphone/turbulence-screen-microphones.html
[13] C.P. VanDercreek, P. Sijtsma, M. Snellen, D. Ragni, F. Avallone, and D.G. Simons, "Deterministic model of acoustic wave propagation in a cavity", AIAA 2019-2425, 25th AIAA/CEAS Aeroacoustics Conference, Delft, The Netherlands, 20-23 May 2019.
[14] C.P. VanDercreek, R. Merino-Martinez, M. Snellen, and D.G. Simons, "Comparison of cavity geometries for a microphone array in an open jet wind tunnel experiment", BeBeC-2020-D7, 8th Berlin Beamforming Conference, 2-3 March 2020.
[15] Virginia Tech Wind Tunnel: http://www.aoe.vt.edu/about/news/articles/news-20150402.html
[16] J. Hurault, A. Gupta, E. Sloth, N.C. Nielsen, A. Borgoltz, and P. Ravetta, "Aeroacoustic wind tunnel experiment for serration design optimisation and its application to a wind turbine rotor", 6th International Meeting on Wind Turbine Noise, Glasgow, UK, 20-23 April 2015.
[17] C.L. Lawson, and R.J. Hanson, *Solving Least Squares Problems*, SIAM, 1995.
[18] R. Merino-Martínez, P. Sijtsma, A. Rubio Carpio, R. Zamponi, S. Luesutthiviboon, A.M.N. Malgoezar, M. Snellen, C. Schram, and D.G. Simons, "Integration methods for distributed sound sources", Int. J. Aeroacoustics, 18 (4-5), 444-469, 2019.
[19] T.F. Brooks, and W.M. Humphreys, Jr., "A deconvolution approach for the mapping of acoustic sources (DAMAS) determined from phased microphone array," J. Sound Vib., 294 (4-5), 856-879, 2006.
[20] P. Sijtsma. "CLEAN based on spatial source coherence", Int. J. Aeroacoustics, 6, 357-374, 2007.
[21] E. Sarradj, G. Herold, P. Sijtsma, R. Merino-Martinez, T.F. Geyer, C.J. Bahr, R. Porteous, D.J. Moreau, and C.J. Doolan, "A microphone array method benchmarking exercise using synthesized input data", AIAA 2017-3719, 23rd AIAA/CEAS Aeroacoustics Conference, Denver, CO, 5-9 June 2017.

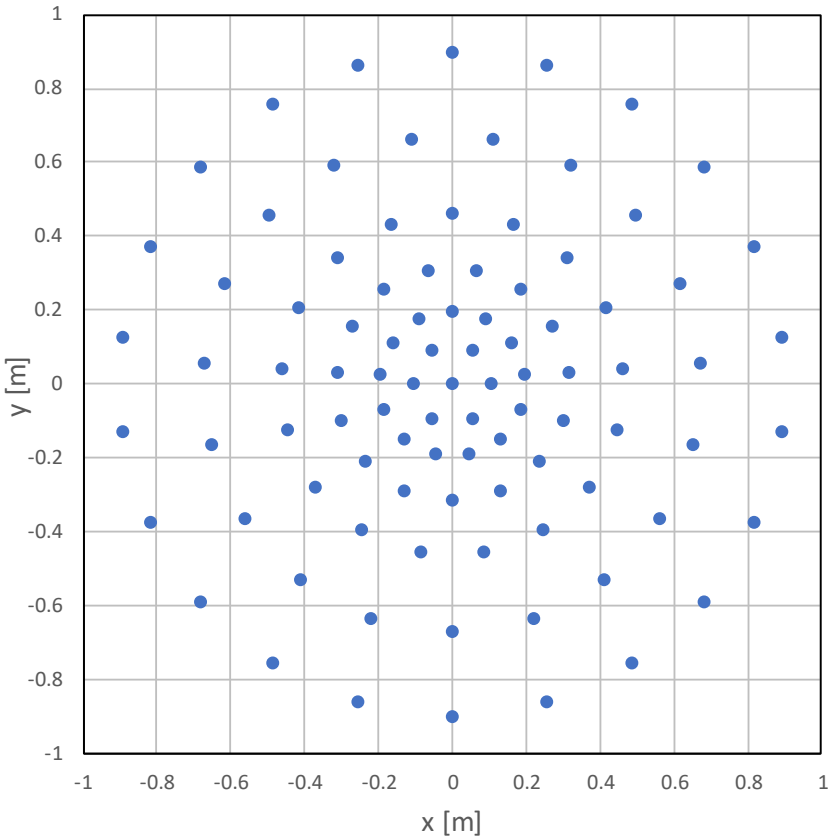

Fig. 1 Array coordinates

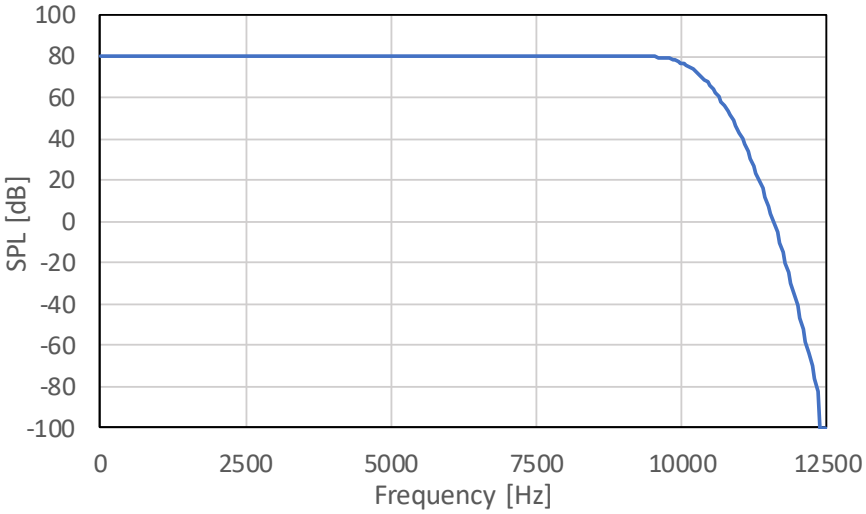

Fig. 2 Target auto-spectrum, 50 Hz bandwidth

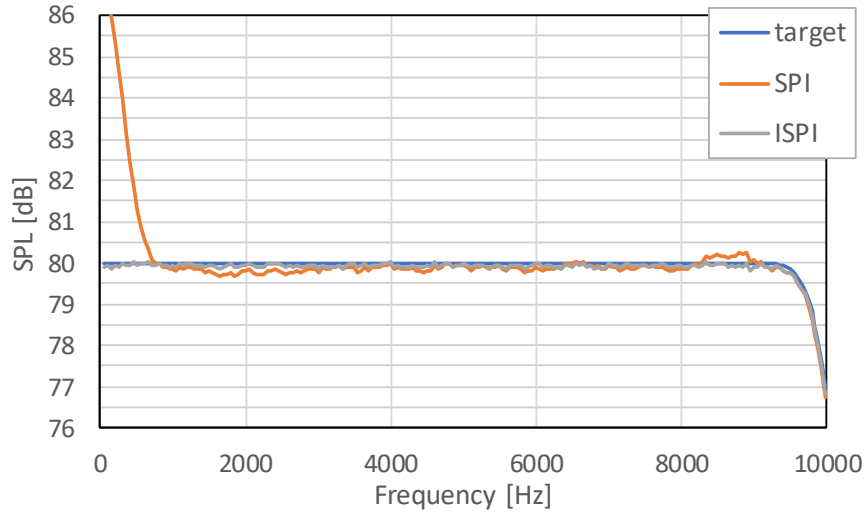

Fig. 3 Integrated results with 5 plane waves and without noise

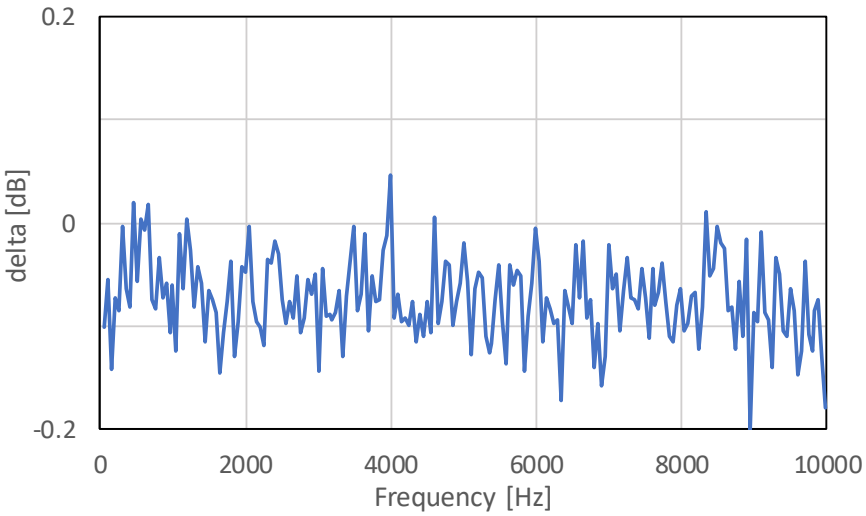

Fig. 4 Difference between ISPI and target spectrum, 5 plane waves, without noise

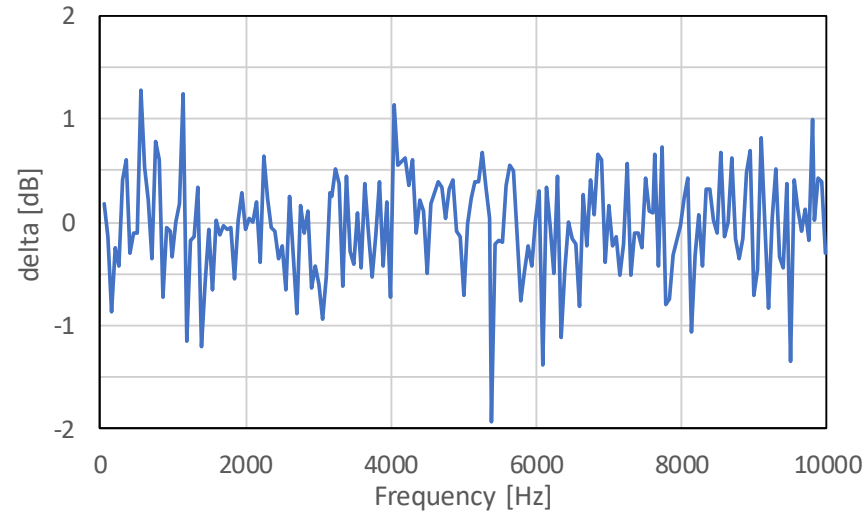

Fig. 5 Difference between ISPI and target spectrum, 5 plane waves, SNR = −23.861 dB

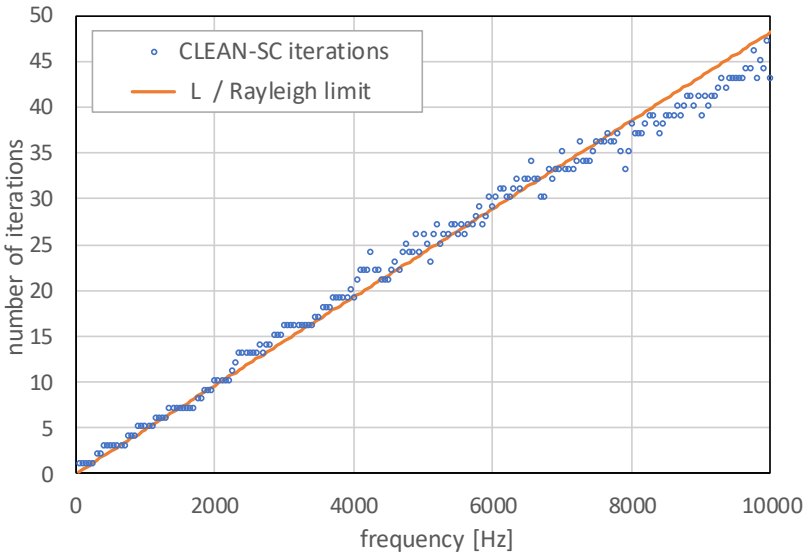

Fig. 6 Estimation of the number of equivalent point sources for a line source

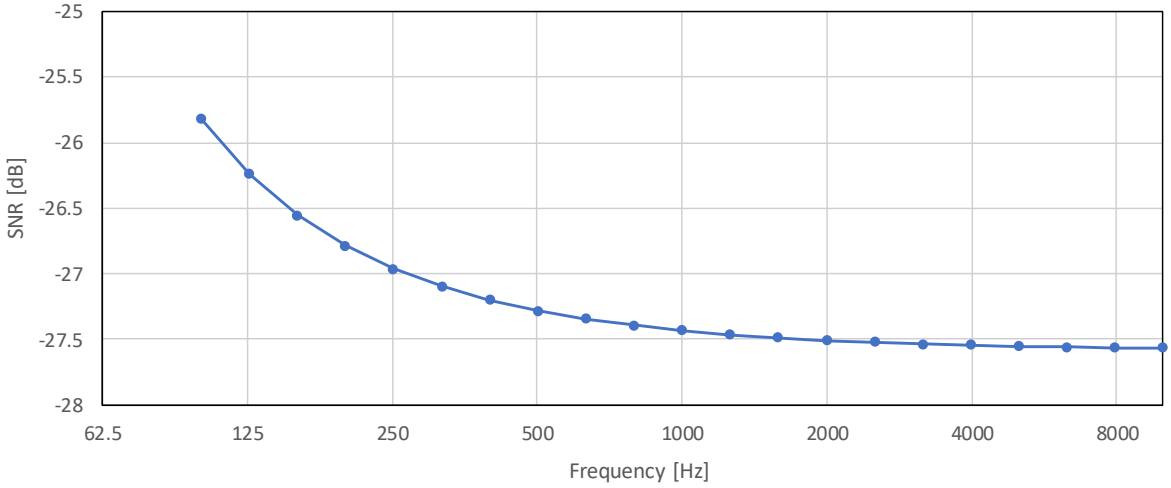

Fig. 7 1/3 octave band SNR threshold

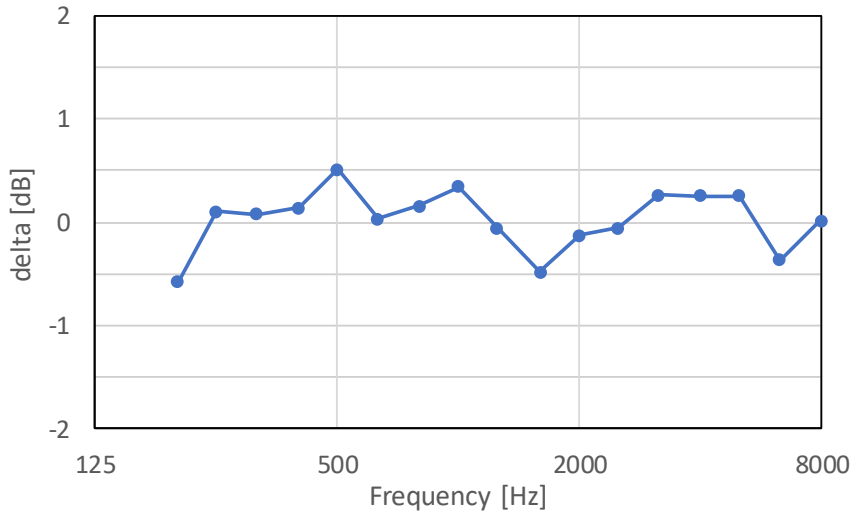

Fig. 8 Difference between SPIL and target spectrum, line source, SNR = −27.433 dB

APPENDIX A: EVALUATION OF FIRST TERM OF EQ. (30)

In this appendix, the first term of Eq. (30) is evaluated. With Eq. (22) we can write

$$I = E\left\{\left(\frac{1}{J}\sum_{k=1}^{K}\sum_{j=1}^{J}\left|a_{k,j}\right|^2 - 1\right)^2\right\} = \frac{1}{J}E\left\{\left(\sum_{k=1}^{K}\left(\left|a_k\right|^2 - \bar{A}_k\right)\right)^2\right\}. \tag{44}$$

The expectation value can be calculated with the joint Gaussian probability density function:

$$I = \frac{1}{J\pi^K}\left(\prod_{k=1}^{k}\bar{A}_k\right)^{=1}\int_{\mathbb{R}^{2K}}\left(\sum_{k=1}^{K}\left(\xi_k^2+\eta_k^2-\bar{A}_k\right)\right)^2\exp\left(-\sum_{l=1}^{K}\frac{\xi_l^2+\eta_l^2}{\bar{A}_l}\right)d\boldsymbol{\xi}d\boldsymbol{\eta}\,, \tag{45}$$

which can be rewritten to

$$I = \frac{1}{J\pi^K}\sum_{k1=1}^{K}\sum_{k2=1}^{K}\bar{A}_{k1}\bar{A}_{k2}\int_{\mathbb{R}^{2K}}\left(\xi_{k1}^2+\eta_{k1}^2-1\right)\left(\xi_{k2}^2+\eta_{k2}^2-1\right)\prod_{l=1}^{K}\exp\left(-\left(\xi_l^2+\eta_l^2\right)\right)d\boldsymbol{\xi}d\boldsymbol{\eta}\,. \tag{46}$$

The terms with $k1 \neq k2$ are zero because

$$\int_{-\infty}^{\infty}\int_{-\infty}^{\infty}\left(\xi^2+\eta^2-1\right)\exp\left(-\left(\xi^2+\eta^2\right)\right)d\xi d\eta = 0\,. \tag{47}$$

Thus, we get

$$I = \frac{1}{J\pi^K}\sum_{k=1}^{K}\bar{A}_k^2\int_{\mathbb{R}^{2K}}\left(\xi_k^2+\eta_k^2-1\right)^2\prod_{l=1}^{K}\exp\left(-\left(\xi_l^2+\eta_l^2\right)\right)d\boldsymbol{\xi}d\boldsymbol{\eta}\,. \tag{48}$$

Since

$$\int_{-\infty}^{\infty}\int_{-\infty}^{\infty}\left(\xi^2+\eta^2-1\right)^2\exp\left(-\left(\xi^2+\eta^2\right)\right)d\xi d\eta = \int_{-\infty}^{\infty}\int_{-\infty}^{\infty}\exp\left(-\left(\xi^2+\eta^2\right)\right)d\xi d\eta = \pi\,, \tag{49}$$

Eq. (48) reduces to

$$I = \frac{1}{J}\sum_{k=1}^{K}\bar{A}_k^2\,. \tag{50}$$